ORIGINAL ARTICLE

The association between genetic variations and morphology-based brain networks changes in Alzheimer's disease

Weixue Xiong[1] | Jiahui Cai[1] | Bo Sun[2] | Henghui Lin[1] | Chiyu Wei[1] | Chengcheng Huang[1] | Xiaohui Zhu[3] | Haizhu Tan[1] | for the Alzheimer' Disease Neuroimaging Initiative

[1]Shantou University Medical College, Shantou, China

[2]Department of Radiology, First Affiliated Hospital of Dalian Medical University, Dalian, China

[3]College of Pharmacy, Shenzhen Technology University, Shenzhen, China

Correspondence
Haizhu Tan, Shantou University Medical College, Shantou, 515000 China.
Email: linnanqia@126.com

Xiaohui Zhu, College of Pharmacy, Shenzhen Technology University, Shenzhen, 518118 China.
Email: zhuxiaohui@sztu.edu.cn

Abstract

Alzheimer's disease (AD) is a highly heritable disease. The morphological changes of cortical cortex (such as, cortical thickness and surface area) in AD always accompany by the change of the functional connectivity to other brain regions and influence the short- and long-range brain network connections, causing functional deficits of AD. In this study, the first hypothesis is that genetic variations might affect morphology-based brain networks, leading to functional deficits; the second hypothesis is that protein–protein interaction (PPI) between the candidate proteins and known interacting proteins to AD might exist and influence AD. 600470 variants and structural magnetic resonance imaging scans from 175 AD patients and 214 healthy controls were obtained from the Alzheimer's Disease Neuroimaging Initiative-1 database. A co-sparse reduced-rank regression model was fit to study the relationship between non-synonymous mutations and morphology-based brain networks. After that, PPIs between selected genes and BACE1, an enzyme that was known to be related to AD, are explored by using molecular dynamics (MD) simulation and co-immunoprecipitation (Co-IP) experiments. Eight genes affecting morphology-based brain networks were identified. The results of MD simulation showed that the PPI between TGM4 and BACE1 was the strongest among them and its interaction was verified by Co-IP. Hence, gene variations influence morphology-based brain networks in AD, leading to functional deficits. This finding, validated by MD simulation and Co-IP, suggests that the effect is robust.

KEYWORDS
Alzheimer's disease, brain morphology, brain network, gene variations, protein–protein interaction

1 | INTRODUCTION

Alzheimer's disease (AD) is the leading cause of dementia globally, and several deficits, such as memory, attention, executive, visuo-spatiality, and language, are observed in patients with AD. More and more previous findings suggest that functional deficits in patients with AD are associated with their underlying brain structure (morphology) (Avila Villanueva et al., 2022). For example, some changed brain morphological features, like reduced cortical thickness and surface area in some brain regions, were related with these deficits (Delbeuck et al., 2003; Thiebaut de Schotten et al., 2011; Yang et al., 2019). After that, the coordinated changes in brain morphology (such as, the visual system components) are found to exist between regions of functional (such as, the visual ability) or anatomical connected systems (Andrews et al., 1997; Zamora-López et al., 2011). However, these studies only focused on the change of a specific brain region's morphology, without considering the function of the brain as an interconnected unity. To describe the brain functional connectivity between structurally and functionally linked brain regions, large-scale brain networks have been identified by leveraging Connectomics to trace functional connectivity (Fauvel et al., 2014; Van Den Heuvel & Pol, 2010). For example, Yeo et al. divided the cerebral cortex into seven brain networks: visual, somatomotor, dorsal motor, ventral attention, limbic, and frontoparietal networks, and the default mode network (DMN) by using the average resting-state fMRI imaging connectivity data from 1000 subjects (Yeo et al., 2011). Based on this, numbers of studies found out that the morphological alternation in the cortical structure of some brain regions are always accompany by the change of the functional connectivity to other brain regions and influence the short- and long-range brain networks connection, causing functional impairments of AD (Fagerholm et al., 2015) (He et al., 2008; Thiebaut de Schotten et al., 2020). Therefore, a tight relationship between brain structure and brain networks might exist (Honey et al., 2007).

While understanding of using the structure and function of brain networks to represent connections between regions is advanced, the potential risk factors that impact brain disconnection and dysfunction remain unexplored in the highly heritable disease AD (Kim et al., 2022; Martens et al., 2022; Stepler et al., 2022). Previous GWAS studies have revealed a bidirectional interplay between the genetic profile and neurological network connectivity (Palk et al., 2020). Chhatwal, J. P. et al. observed alterations in DMN connectivity in both symptomatic and asymptomatic carriers of pathogenic mutations of presenilin-1, presenilin-2, and amyloid precursor protein (APP) (Chhatwal et al., 2013). The clusterin gene has been reported to consistently affect the changing patterns of the DMN in subjects at high risk of AD (Ye et al., 2017). However, structural and brain network changes are analyzed separately in most of these studies. Hence, after constructing the large-scale brain networks by using some brain morphological features from MRI, we firstly hypothesis that genetic variations might act on the brain functional connectivity across brain regions are introduced in our study.

To determine the molecular structure-to-function of the potential proteins in AD, dynamics and structure of proteins from molecular dynamics (MD) simulation can be further analyzed by applying the protein–protein interactions (PPIs) which is inferred by using information from known interacting proteins to AD (Chong et al., 2021). More than 80% of PPIs are established to construct metabolic and signal pathways to get functions (Keskin et al., 2016). Dysfunction and malfunction of pathways and alterations in PPIs have shown to be related to some diseases, like neurodegenerative disease (Keskin et al., 2016). β-site APP-cleaving enzyme-1 (BACE1) hydrolyzes amyloid precursor protein (APP) to produce Aβ42, a protein known to correlate with the degree of dementia (Wang et al., 2018), such as AD (Armstrong et al., 2019; Buchete & Hummer, 2007; Vagnoni et al., 2012). PPIs between BACE1 and the nuclear factor kappa-B (NF-κB) are established to oxidative stress and inflammatory responses in AD by enhancing BACE1 transactivation and were found to promote amyloid production in Wang Yi-Bin and Gurdeep Marwarha (Marwarha et al., 2018; Yi-Bin et al., 2022). Hence, the second hypothesis of our study is that PPIs between the candidate proteins and BACE1 may exist. Methods including modeling, docking and MD simulation are accurate and reliable approaches to evaluate the functional relevance of the predicted PPIs and the prediction of their realistic binding affinity. Nevertheless, using the follow-up experiments like co-immunoprecipitation (Co-IP) to further validate the results of the PPIs is indispensable.

According to these two hypothesis, genes with non-synonymous mutations were screened before splitting the cerebral cortex into seven brain networks using structural magnetic resonance imaging scans. The co-sparse reduced-rank regression (CSRRR) method is then applied to detect the impact of selected genes on the corresponding brain network. Homology modeling, molecular docking, MD simulations, and Co-IP, are also performed to reveal the biological mechanisms underlying AD.

2 | METHODS

2.1 | Data collection

Accelerated T1-weighted structural MRI scans with 1.5 T scanners and approximately 600 470 variants on chromosome 1–22 in 175 patients with AD and 214 healthy controls (HCs) from the ADNI-1 datasets (http://adni.loni.usc.edu/). The investigators within the ADNI provided the data but did not participate in analysis or writing of this manuscript. Information about written informed or phone consent, all relevant ethical guidelines and/or ethics committee approvals, and policies about blind were seen in the ADNI-1 dataset. According to the ADNI data generation policy, samples were collected using blinding and only unblinded when uploaded to databases (https://adni.loni.usc.edu/wp-content/themes/fresh news-dev-v2/documents/clinical/ADNI-1_Protocol.pdf). All project team members were blinded to the participant IDs in ADNI

(Zicha et al., 2022). Thus, experimental data were not linked to demographic, clinical, or other biomarker data for the participants until after the experimental data were uploaded to the ADNI website (Rowe et al., 2021). Sample sizes were estimated based on comparable previously published literature (Hu et al., 2018). The power analysis sample size (PASS) estimation of the study was performed using PASS software. We calculated with alpha set at 0.05 that 28 patients per group would give a statistical power of 90% to detect an 18.4 difference in the population mean difference between the groups. One hundred and seventy-five patients with AD and 214 HC were recruited because of the possibility of dropouts and all the samples met the selection criteria.

2.2 | Participants

The two-sample Kolmogorov–Smirnov test was used to test whether the data follow the normal distribution. The method of the Levene's test was adopted to check the homogeneity of variance. The collinearity and mis-measured outliers were handled by considering the results of variance inflation factor (VIF) and minimum covariance determinant (MCD). To compare the difference of demographic characteristics and morphology-based brain networks between two groups, several two-sided parametric or non-parametric difference analyses were performed due to the distribution of the data.

2.3 | Data pre-processing

2.3.1 | Genetic data pre-processing

Several preliminary procedures were carried out, including quality control (QC), the conversion of genome coordinates into hg19, phasing, and imputation on the Michigan imputation server (a web-based imputation service that facilitates access to new reference panels, https://imputationserver.sph.umich.edu/index.html#!pages/home). Imputed single nucleotide polymorphisms (SNPs) with an $R^2 < 0.8$ were identified using BCFTOOLS (a set of tools that manipulate variant calls in the Variant Call Format and Binary Call Format). SNPs with a SNP call rate above 0.05, samples with a call rate higher than 0.05, rare variants and low frequency variants (minor allele frequency < 5%), and SNPs with a disrupted Hardy–Weinberg equilibrium (p-value $< 1 \times 10^{-5}$), were removed in the quality control step (Laurie et al., 2010). ANNOVAR (Annotate Variation), an efficient software tool to functionally annotate genetic variants detected from diverse genomes (http://www.openbioinformatics.org/annovar/), was then used to perform gene functional annotation to retain non-synonymous mutations (Carlton et al., 2006). Principal component analysis was also performed using the EIGENSTRAT tool, a popular association mapping method with good power and type I error control (Price et al., 2006).

2.3.2 | Imaging data pre-processing

T1-weighted images underwent a series of automatic image processing steps using FreeSurfer software (version 6.0, https://surfer.nmr.mgh.harvard.edu/). All data files were first converted into a compressed Massachusetts General Hospital file (MGZ) format. Then, a 30-step pre-processing, involving skull stripping, intensity normalization, white matter segmentation, and reconstruction of brain morphology including the internal and external cortical surface, was performed. Data from one subject with a low-quality segmented white matter image were excluded. According to Yeo et al.'s functional network atlas, seven brain networks including visual, somatomotor, dorsal attention, ventral attention, limbic, frontoparietal control, and DMN were obtained. Resting-state network relating to cortical thickness and surface area was finally extracted.

2.4 | Statistical analysis

2.4.1 | Association analysis between imaging phenotypes and genetic variants

Each network-based cortical thickness and network-based surface area were separately adjusted in linear regression to control for potential confounders, including age, sex, apolipoprotein E epsilon 4 allele (APOE4), and significant principal components (PCs) which were calculated by principal component analysis (PCA) (Gauch Jr et al., 2019). To investigate the association with genetic variants and imaging phenotypes between AD and HC cohorts, the CSRRR model (Wen et al., 2020) was applied to efficiently and precisely detect simultaneously high-dimensional genetic variants (independent variables) and imaging phenotypes (dependent variables) via non-convex penalty. Next, a simple linear regression was fitted for each individual SNP to determine which brain network it most likely contributes to. In this step, the Bonferroni correction p-value was set to 0.05/number of comparison tests performed.

2.4.2 | The effect analysis of the strongest PPI candidate gene on morphology-based brain network

To further explore how the selected significant SNP impacted on the significant brain network and brain morphology, several two-sided parametric or non-parametric difference analyses were performed including the difference of brain network and brain morphology between homozygous group and heterozygous group; the difference of brain network and brain morphology between AD and HC cohort in homozygous group or heterozygous group; the difference of brain network and brain morphology between homozygous group and heterozygous group in AD or HC cohort.

A value of *p* less than 0.05 was considered to be statistically significant in all analyses. All the statistical analyses were carried out using the R (version 4.1.1).

2.5 | Experimental validation of computational biology and cell biology

2.5.1 | Molecular dynamic simulation

The quality of the predicted protein structures was evaluated using PROCHECK (Laskowski et al., 1993) and ROSA (Wiederstein & Sippl, 2007) programs. The I-TASSER server (Yang et al., 2015) was used to model the full-length predicted protein structures, and target amino acids were mutated using Chimera 1.14 (Pettersen et al., 2004). Docking proteins were assessed using High Ambiguity Driven protein–protein Docking (Dominguez et al., 2003). MD was carried out before neutralizing the system using GROMACS 2020.3 (https://manual.gromacs.org/documentation/2020.3/release-notes/2020/2020.3.html). Next, we selected the OPLS-AA/L all-atom force field and the cube box, set the distance from the boundaries of the box, adjust NVT and NPT balance, and release the location restrictions. Finally, 50 ns procedures were implemented. The root mean square deviation, radius of gyration, solvent accessible surface area, and number of hydrogen bonds, were measured to assess system balance and compare the results of native and mutant protein structures. To determine the binding affinity of protein complexes, the overall High Ambiguity Driven protein–protein Docking score was used (Dominguez et al., 2003). And a lower score represents stronger binding affinity. Buried surface area (BSA), commonly used to measure how well a protein complex was protected from exposure to the outer system, indicated that PPIs were stronger while interaction while the BSA was higher (Gopalakrishnan et al., 2019).

2.5.2 | Co-immunoprecipitation experiment

According to the certificate of analysis, HEK 293T cells (Cat: CRL-11268) obtained from the ATCC had a maximum passage number of 50. HEK293T cell line was not listed as a commonly misidentified cell line by the International Cell Line Authentication Committee. HEK293T cell line was always identified by short tandem repeat (STR) technology. HEK 293T cell line (RRID:CVCL_4U22), Anti-Flag antibody (Antibodies-Online Cat# ABIN349610, RRID:AB_10771694), HA-Tag antibody (Vanderbilt Antibody and Protein Resource Cat# Anti-HA 12CA5, RRID:AB_2923038), Anti-Flag magnetic beads (RRID:CVCL_4U22), Anti-HA magnetic beads (MBL International Cat# M132-9, RRID:AB_10693554).

HEK 293T cells for protein extraction were transfected with both pcDNA3.1 (+)-Flag-BACE1 and pcDNA3.1 (+)-HA-transglutaminase 4 (TGM4). Forty-eight hours after transfection, HEK 293T cells were harvested by scraping cells into NP-40 lysis buffer after gently washing twice with pre-chilled PBS (5 min per wash), and were then subjected to Co-IP assay. After incubation, cells were centrifuged and the supernatant was immediately transferred to a fresh tube. After quantifying and diluting the total protein concentration, the cells were incubated overnight at 4°C with anti-Flag (or anti-HA) magnetic beads. Samples were washed three times after each incubation step. To terminate the reactions, 1 × sodium dodecyl sulfate (SDS) loading buffer was added and boiled for 5 min. Lysates are then subjected to SDS polyacrylamide gel electrophoresis (SDS-PAGE) and transferred to polyvinylidene fluoride membranes. The immunoprecipitated proteins and their binding partners are separated by SDS-PAGE for western blot analysis. After preparing membranes, autoradiography signals are detected by enhanced chemiluminescence.

3 | RESULTS

3.1 | Sample characteristics

The results of Kolmogorov–Smirnov test displayed that age did not follow the normal distribution in AD (df = 148, D = 0.0762, *p*-value = 0.352) and HC (df = 179, D = 0.105, *p*-value = 0.036) groups. The results of Levene's test suggested that age did not fulfill the homogeneity of variance assumption (df = 327, F = 31.595, *p*-value = 4.073 E-08). As shown in Table S1, the result of VIF indicated that there was no collinearity between variables. No outlier was existed according to the results of MCD. As shown in Table 1, the results of difference analysis between the AD and HC cohorts showed that no differences in sex (df = 1, χ^2 = 0, *p*-value = 0.907), age (df = 387, χ^2 = 18 983, *p*-value = 0.815), and race (df = 3, Fisher's Exact, *p*-value = 0.357) were existed. APOE4, an important genetic biomarker for AD pathophysiology, was significantly different between the AD and HC (df = 2, χ^2 = 68.783, *p*-value<0.001).

In addition, Table S2 also described the results of difference analysis on morphology-based networks between two groups. For example, no significant differences of visual network in left surface area were observed in AD patients while compared to the HCs (df = 327, *t* = −1.619, *p*-value = 0.106), and significant differences of visual network in right surface area between two groups were found (df = 327, *t* = −2.582, *p*-value<0.05).

3.2 | Genetic data and imaging data pre-processing

After genetic pre-processing, we retained 11 596 SNPs in 150 AD samples and 180 HCs. Six significant PCs were introduced as additional variables.

One sample was removed because of the low quality of the segmented white matter image. Following the identification of seven main functional cortical networks in each hemisphere, 14 network-based measures of cortical thickness and 14 network-based measures of surface area were extracted.

TABLE 1 Comparisons of demographics and clinical variables between AD and HC cohorts

	AD	HC	Df	Test statistics	p-value
No. of participants, n (%)	175 (45%)	214 (55%)			
Sex, n (%)					
M	93 (53%)	115 (54%)	1	0	0.907
F	82 (47%)	99 (46%)			
Age, Median (IQR)	75.8 (70.85, 81.10)	75.5 (72.12, 78.38)	387	18 983	0.815
Race, n (%)					
Asian	2 (1)	2 (1)	3	Fisher's Exact	0.357
Black	8 (5)	15 (7)			
More than one	2 (1)	0 (0)			
White	163 (93)	197 (92)			
APOE4, n (%)					
0	58 (33)	156 (73)	2	68.783	<0.001
1	85 (49)	53 (25)			
2	32 (18)	5 (2)			

Note: APOE4 was coded as the number of epsilon 4 alleles (0, 1, or 2). Degrees of freedom (df).

TABLE 2 Significant results of CSRRR for cortical thickness

Gene_Name	rs_number	Variant_ID	Network_Name
ADAMTS5	rs2830585	21-28 305 212-C-T	Visual (L)
ADAMTS5	rs2830585	21-28 305 212-C-T	Dorsal attention (L)
ADAMTS5	rs2830585	21-28 305 212-C-T	Dorsal attention (R)
ADAMTS5	rs2830585	21-28 305 212-C-T	Visual (R)
ADAMTS5	rs2830585	21-28 305 212-C-T	Frontoparietal (R)
ADAMTS5	rs2830585	21-28 305 212-C-T	Ventral attention (R)
ADAMTS5	rs2830585	21-28 305 212-C-T	default mode (L)
TGM4	rs1395388	3-44 948 674-G-C	Visual (L)
RNF212	rs616196	4-1 087 393-G-T	Frontoparietal (R)
RNF212	rs615381	4-1 087 531-T-C	Frontoparietal (R)
RNF212	rs614945	4-1 087 617-C-A	Frontoparietal (R)
SLC1A4	rs759458	2-65 245 365-G-A	Ventral attention (R)
CCDC186	rs7095762	10-115 910 928-G-T	Dorsal attention (L)
CCDC186	rs1061159	10-115 922 774-G-A	Dorsal attention (L)
TGM4	rs1395388	3-44 948 674-G-C	Visual (R)
CCDC186	rs7095762	10-115 910 928-G-T	Visual (L)
CCDC186	rs1061159	10-115 922 774-G-A	Visual (L)

Note: CSRRR: Co-sparse reduced-rank regression. L: left hemisphere. R: right hemisphere.

3.3 | Association between imaging phenotypes and genetic variants

We identified five genetic risk factors that influenced brain networks with regards to cortical thickness measurements: *ADAMTS5*, *TGM4*, *RNF212*, *SLC1A4*, and *CCDC186* (see Table 2 and Figure 1a). Figure 1b described the association of TGM4 with the visual network.

For the network-based surface area, three genetic risk factors including *ARMC3*, *ANKRD33*, and *F5* were found to affect brain networks (somatomotor, ventral attention, frontoparietal, default mode, somatomor) (see Table 3 and Figure 2a). Figure 2b depicted the association of ARMC3 with several brain networks (right somatomotor, left somatomotor, left ventral attention, right ventral attention, right frontoparietal, right default mode, left default mode).
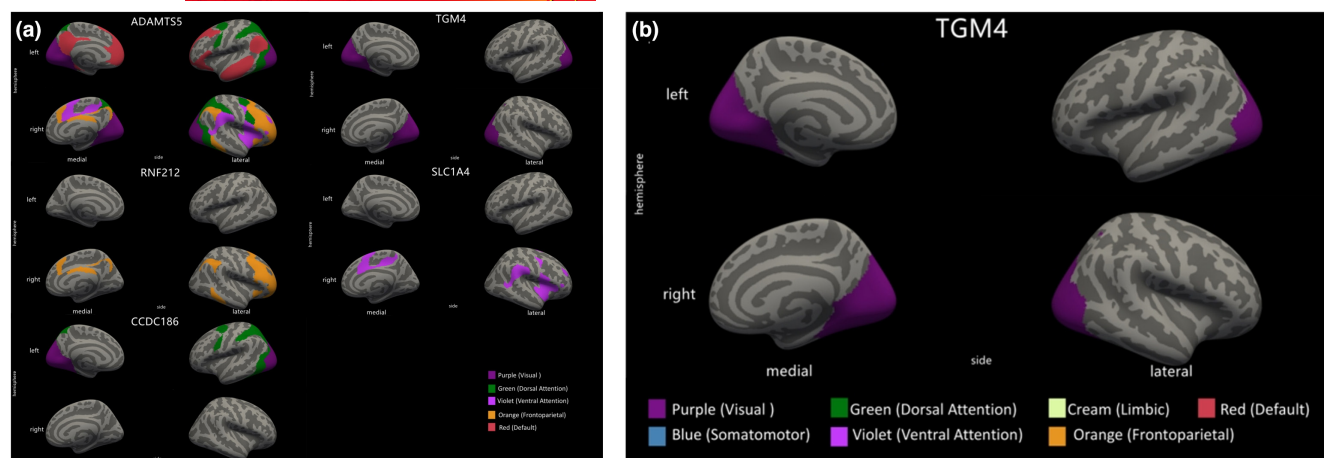
FIGURE 1 The association between imaging phenotypes extracted from cortical thickness measurements and genetic variants. (*n* = 329 participants). (a) The relationship between five genetic risk factors and brain networks. (b) The association of TGM4 with the visual network.

TABLE 3 Significant results of CSRRR for surface area

Gene_Name	rs_number	Variant_ID	Network_Name
ARMC3	rs10828395	10-23 297 252-G-A	Somatomotor (R)
ARMC3	rs10828395	10-23 297 252-G-A	Somatomotor (L)
ARMC3	rs10828395	10-23 297 252-G-A	Ventral attention (L)
ARMC3	rs10828395	10-23 297 252-G-A	Ventral attention (R)
ARMC3	rs10828395	10-23 297 252-G-A	Frontoparietal (R)
ARMC3	rs10828395	10-23 297 252-G-A	Default mode (R)
ARMC3	rs10828395	10-23 297 252-G-A	Default mode (L)
ANKRD33	rs34494292	12-52 284 500-A-G	Somatomotor (L)
ANKRD33	rs3180417	12-52 285 086-G-A	Somatomotor (L)
F5	rs6032	1-169 511 555-T-C	Default mode (L)
F5	rs4525	1-169 511 734-T-C	Default mode (L)
F5	rs4524	1-169 511 755-T-C	Default mode (L)

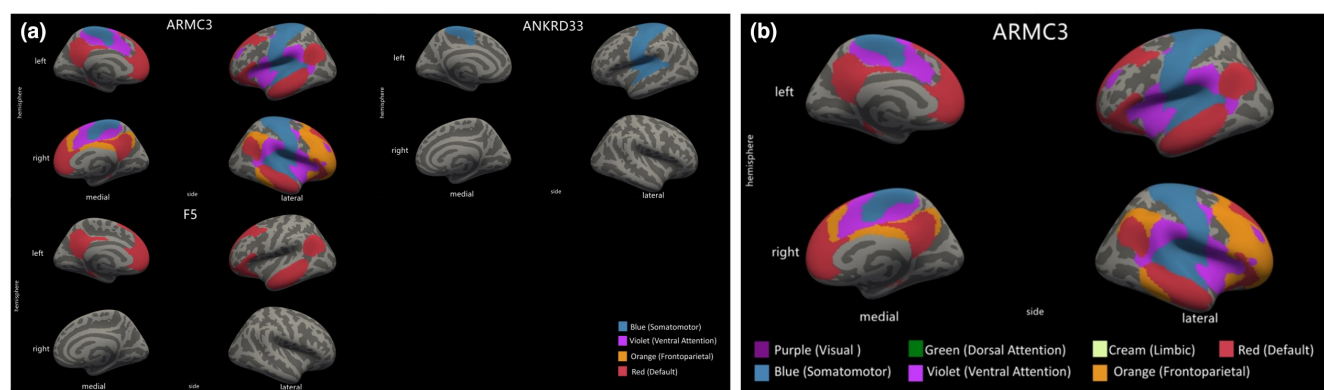*Note*: CSRRR: Co-sparse reduced-rank regression. L: left hemisphere. R: right hemisphere.

FIGURE 2 The association between imaging phenotypes extracted from surface area and genetic variants. (*n* = 329 participants). (a) The relationship between three genetic risk factors and brain networks. (b) The association of ARMC3 with several brain networks.

3.4 | Docking and molecular dynamics simulations of the selected BACE1 complex of SNPs

Table 4 presented the docking results of the interactions of the selected proteins (TGM4, RNF212, ANKRD33) with BACE1. For example, the Van der Waals interaction between TGM4 and BACE1 for the native complexes was -22.1 ± 20.1 Kcal/mol^{-1}, while for the mutant Glu437Gln (rs1395388), the Van der Waals interaction was -30.3 ± 17.4 Kcal/mol^{-1}. Compared to the native Glu437Gln, the electrostatic interaction was lower in the mutant Glu437Gln (-229.5 ± 68.1 Kcal/mol^{-1} vs. -210.7 ± 41.1 Kcal/mol^{-1}). For the native complex of TGM4, the BSA value was 3724.4 ± 277.5 A$^{\circ 2}$, while compared to 3622.4 ± 259.5 A$^{\circ 2}$ in the mutant Glu437Gln. Furthermore, the energy which was required to separate the complexes (the desolvation energy) was higher in the native complex of RNF212 (-30.1 ± 2.8 Kcal/mol^{-1}) but lower in the mutant Gln173Arg (-25.0 ± 4.9 Kcal/mol^{-1}).

Figure 3 described the docking results of the interactions of selected proteins with BACE1 which indicated that a potential interaction of BACE1 with the mature catalytic region (46–460) in the TGM4. The docking analysis revealed that PPIs between wild-type ANKRD33 and BACE1 were stronger than the PPIs between mutant Val261Ile and BACE1. A potential explanation was that the electrostatic energy and BSA of wild-type ANKRD33 were lower than that of its mutant Val261Ile. Meanwhile, the higher desolvation energy of the wild-type RNF212 complex caused a higher PPIs between wild-type RNF212 and BACE1 than that of its mutant Gln173Arg with BACE1 (Gopalakrishnan et al., 2019).

The root mean square deviation (RMSD) plot revealed that there were no erratic fluctuations in the molecular systems and that all complexes were stable (Figure 4a). The radius of gyration results revealed that a volumetric and compactness variation was induced by the complex (Figure 4b). The solvent accessible surface area results for the protein structures indicated a dimensional discrepancy (Figure 4c). The hydrogen bond results accounted for the proteins' rigidity and their ability to interact with partners (Figure 4d). Molecular dynamics simulation results of interactions between ANKRD33 and RNF212 and BACE1, respectively, are shown in the Supplementary Material (Figures S7 and S8). Consequently, TGM4 (NP_003232.2) was selected for the subsequent Co-IP experiment, because it had the strongest interaction with BACE1.

3.5 | Co-immunoprecipitation

SDS-PAGE analysis detected a band for HA-TGM4 in the pull-down complex. Furthermore, when using a Flag rabbit polyclonal antibody, a Flag-BACE1 band was checked in the pull-down complex

TABLE 4 The docking results of the interactions of selected proteins with BACE1

	BACE1_ANKRD33	BACE1_RNF212	BACE1_TGM4
HADDOCK score	-16.1 ± 10.9	-4.9 ± 7.4	-22.1 ± 20.1
RMSD from the overall lowest-energy structure	24.7 ± 0.6	0.7 ± 0.4	1.1 ± 0.9
Van der Waals energy, Kcal/mol^{-1}	-86.1 ± 8.1	-92.8 ± 4.5	-119.2 ± 12.4
Electrostatic energy, Kcal/mol^{-1}	-287.4 ± 41.2	-217.8 ± 25.1	-229.5 ± 68.1
Desolvation energy, Kcal/mol^{-1}	-2.4 ± 3.5	-30.1 ± 2.8	-1.3 ± 5.2
Buried Surface Area, A$^{\circ 2}$	2557.1 ± 109.2	3200 ± 53.7	3724.4 ± 277.5
Z-Score	-1.3	-1.5	-2.3
	BACE1_ANKRD33 Val261Ile	**BACE1_RNF212 Gln173Arg**	**BACE1_TGM4 Glu437Gln**
HADDOCK score	-16.0 ± 5.6	-14.5 ± 11.9	-30.3 ± 17.4
RMSD from the overall lowest-energy structure	15.0 ± 0.3	0.6 ± 0.4	1.1 ± 0.9
Van der Waals energy, Kcal/mol^{-1}	-81.8 ± 1.9	-105.0 ± 4.7	-113.7 ± 13.7
Electrostatic energy, Kcal/mol^{-1}	-139.0 ± 22.9	-190.4 ± 16.3	-210.7 ± 41.1
Desolvation energy, Kcal/mol^{-1}	-20.0 ± 3.8	-25.0 ± 4.9	-2.2 ± 6.8
Buried Surface Area, A$^{\circ 2}$	2612.4 ± 113.3	3705.4 ± 30.5	3622.4 ± 259.5
Z-Score	-0.9	-2	-2.5

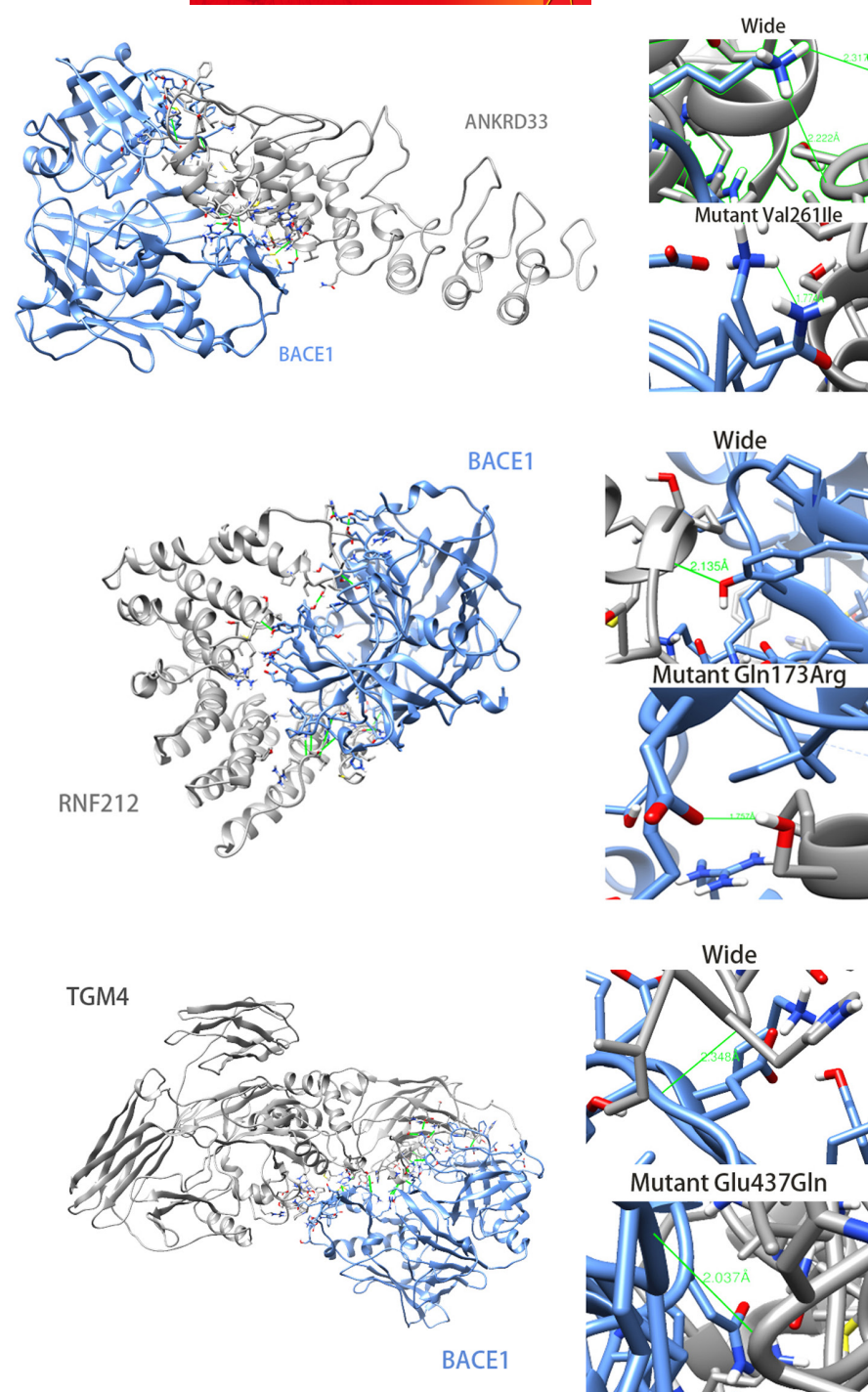*Note*: CSRRR: Co-sparse reduced-rank regression. L: left hemisphere. R: right hemisphere.

FIGURE 3 The docking results of selected proteins with BACE1 (*n* = 3 different proteins).

(Figure 5). These findings provided evidence for PPIs between BACE1 and TGM4.

3.6 | The effect analysis of the strongest PPI candidate gene on morphology-based brain network

The results of the difference of morphology-based brain network between homozygous group and heterozygous group suggested that homozygous individuals had smaller visual network cortical thickness volume in left and right hemisphere than that of heterozygous individuals (Figure 6A, df = 327, bd.constant$_{left}$ = 0.0421, *p* = 0.01; bd.constant$_{right}$ = 0.0188, *p* = 0.07). The results of the difference of morphology-based brain network between AD and HC cohort in homozygous group indicated that cortical thickness in both left and right visual networks of AD was different from that of HC (top of Figure 6B, df = 280, χ^2_{left} = 5967.5, *p* < 0.001; χ^2_{right} = 5618, *p* < 0.001). The results of the difference of morphology-based brain network between AD and HC cohort in heterozygous group showed that cortical thickness in the right visual networks of AD differed from that of HC (bottom of Figure 6B, df = 44, *t* = −2.281, *p* = 0.03). The
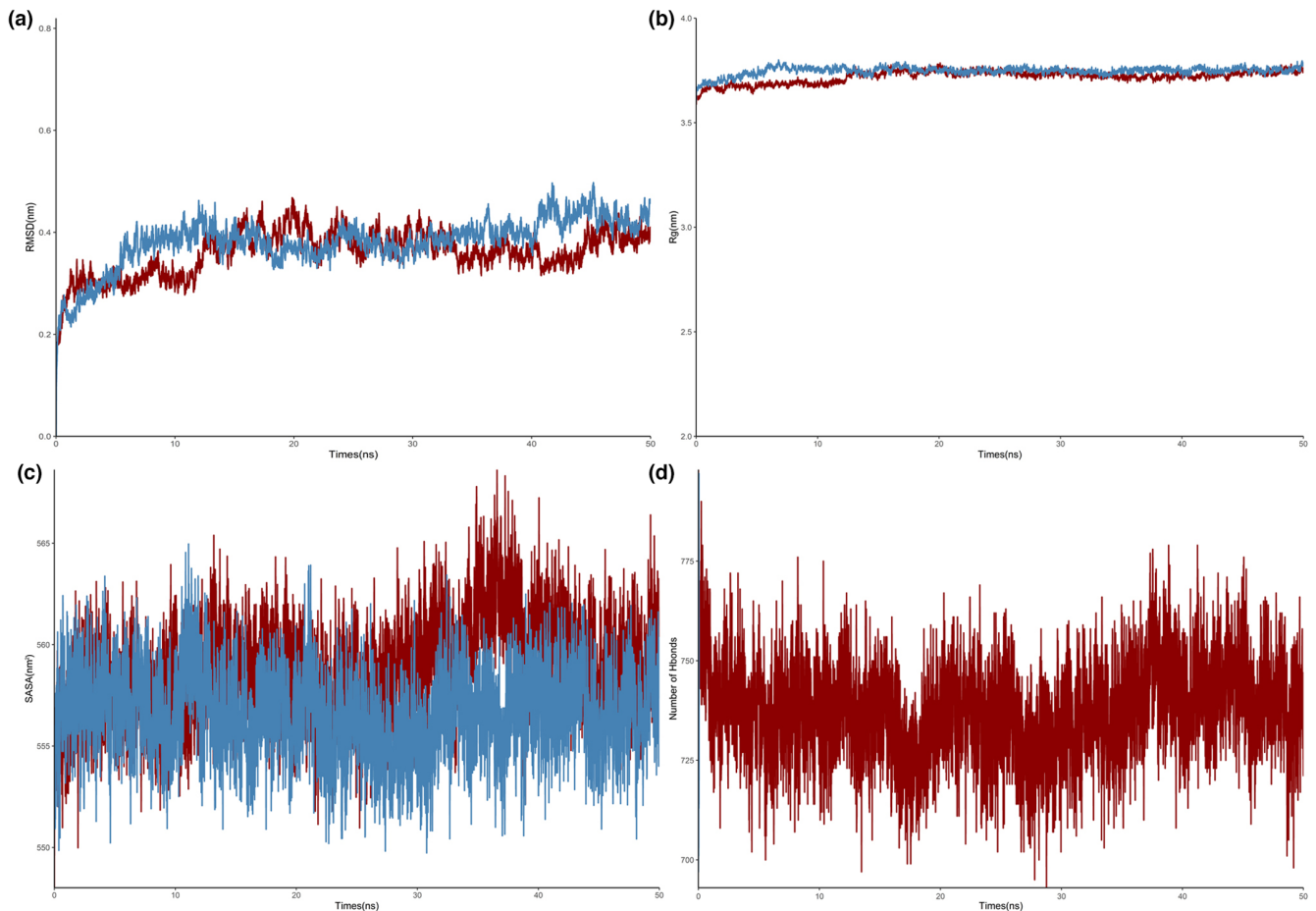
FIGURE 4 The MD results for TGM4 wild-type (blue line) and TGM4 mutants (red line). (a: RMSD plot revealed that all complexes were stable after 15 ns. b: Rg plots showed higher Rg in mutants than in wild-type in 10–30 ns. c: shows SASA variations observed during 50 ns. d: shows H-bonds variations observed during 50 ns. $n = 1$ BACE_TGM4 protein complex).

results of the difference of morphology-based brain network between homozygous group and heterozygous group in AD displayed that cortical thickness in the left visual networks of patients with homozygous was different from that of patients with heterozygous (top of Figure 6C, df = 147, bd.constant = 0.0800, $p = 0.03$). The results of the difference of morphology-based brain network between homozygous group and heterozygous group in HC cohort suggested that there was no significant difference of cortical thickness in visual network between two groups (bottom of Figure 6C, df = 177, $bd.constant_{left} = 0.0259$, $p > 0.05$; $bd.constant_{right} = 0.0165$, $p > 0.05$).

Some other significant different brain networks in other brain regions are depicted in Figure 6D. Furthermore, detailed difference analysis results are displayed in the supplementary material (Tables S3–S7).

4 | DISCUSSION

The results of our morphology-based brain networks analysis showed TGM4, DAMTS-5, RNF212, CCDC186, and SLC1A4 had influence

on five cortical thickness-based brain networks (the visual network, DMN, dorsal attention network, ventral attention network, and frontoparietal control network). Four cortical surface brain networks (the somatomotor network, ventral attention network, frontoparietal control network, and DMN) were also influenced by ARMC3, ANKRD33, and F5. Most of these results were coincident with some previous studies (Bajaj et al., 2017; Palaniyappan et al., 2020; Zhao et al., 2022). For example, RNF112 and ANKRD32 are identified by Walker, R.L. et al. (Walker et al., 2019) and Zhao et al. (Zhao et al., 2022), showing these genes play key roles in biology process of brain development and healthy aging (Zhao et al., 2022). Likewise, these results are coincided with our study because RNF112 and RNF212 belong to the same family, so do ANKRD32 and ANKRD33.

MD simulations have succeeded in revealing the mechanisms of protein aggregation associated with neurodegenerative disorders (Hollingsworth & Dror, 2018). Moreover, combing MD simulation and Co-IP experiment is a valuable way to explore molecular properties which are difficult or impossible to investigate only by some wet-laboratory experiments. In the present study, homology modeling, molecular docking, and MD simulation results suggested that TGM4, RNF212, and ANKRD33 exhibits functional interactions
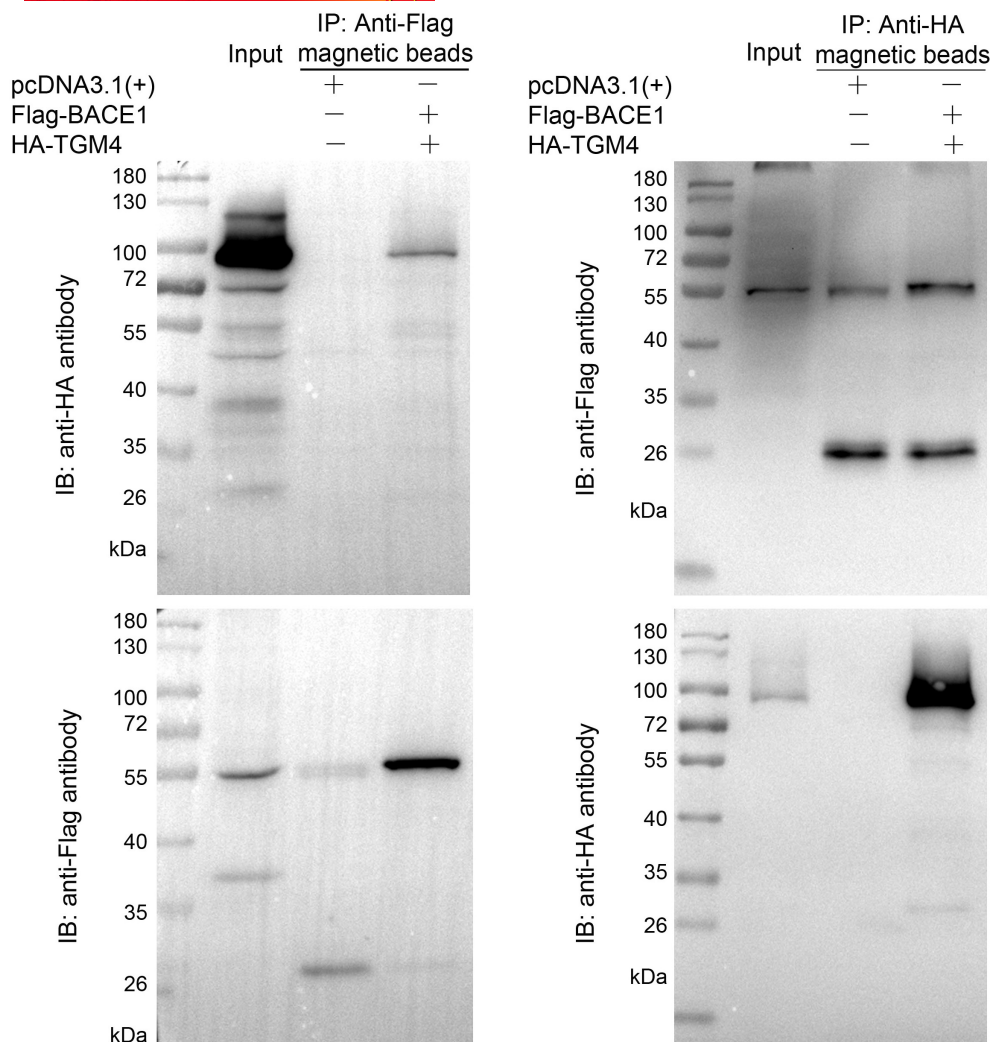
FIGURE 5 SDS-PAGE results showing the interaction between TGM4 and BACE1 (maximum number of passages: $n = 50$).

with BACE1. The bioinformatics analysis provides insight into the act of these interactions on certain brain regions. For example, TGM4 (Transglutaminase-4) is a member of transglutaminase family which may contribute to amyloid deposition in the insula of cerebral cortex in Alzheimer's disease (Dudek & Johnson, 1994; Gentile et al., 1995). RNF212 can encode an E3 enzyme in the ubiquitin proteasome system whose dysfunction could lead to Aβ accumulation in basal ganglia, cerebral cortex, hippocampal, and amygdala (Wang et al., 2021). ANKRD33 has been described to be involved in a variety of functions, such as cell–cell signaling and cytoskeleton structure in cerebral cortex and retina (Rostamirad, 2010). These results indicated that these genes could affect Aβ production by altering and regulating BACE1 activity, and spatial patterns of Aβ deposition in AD patients affect brain network function. In addition, TGM4 showed the strongest PPIs with BACE1 and its interaction was further confirmed by Co-IP experiments. This suggests that TGM4 may mediate the remodeling of the extracellular matrix (ECM) and stiffen the vessel wall through interacts with BACE1, a structure that connects the ECM and cleaves APP to produce Aβ (Farris et al., 2021; Tan et al., 2020; Theocharis et al., 2016; Zhang & Song, 2013), thus resulting in an

impaired clearance of Aβ from the brain and leading to brain atrophy (Jellinger & Attems, 2005; Wilhelmus et al., 2012). This is consistent with study of De Jager et al. (de Jager et al., 2013).

5 | LIMITATIONS AND FUTURE DIRECTIONS

A noteworthy limitation of this study was that only BACE1 was selected as the known interacting protein in MD simulation and Co-IP experiments. If other AD-related proteins besides BACE1, for example, ApoE or presenilin, are introduced, it might be possible to identify more genes that are involved in AD. Inconsistencies in types of the MRI scanner across laboratory centers and the small sample size are also the limitation in our study.

Series studies on morphology-based brain networks analysis, MD simulation, and CO-IP experiments were preliminary. Although further validation studies including animal experiments and clinical trials are beyond our expertise, it is very important for us to learn how to deal with them in the future.
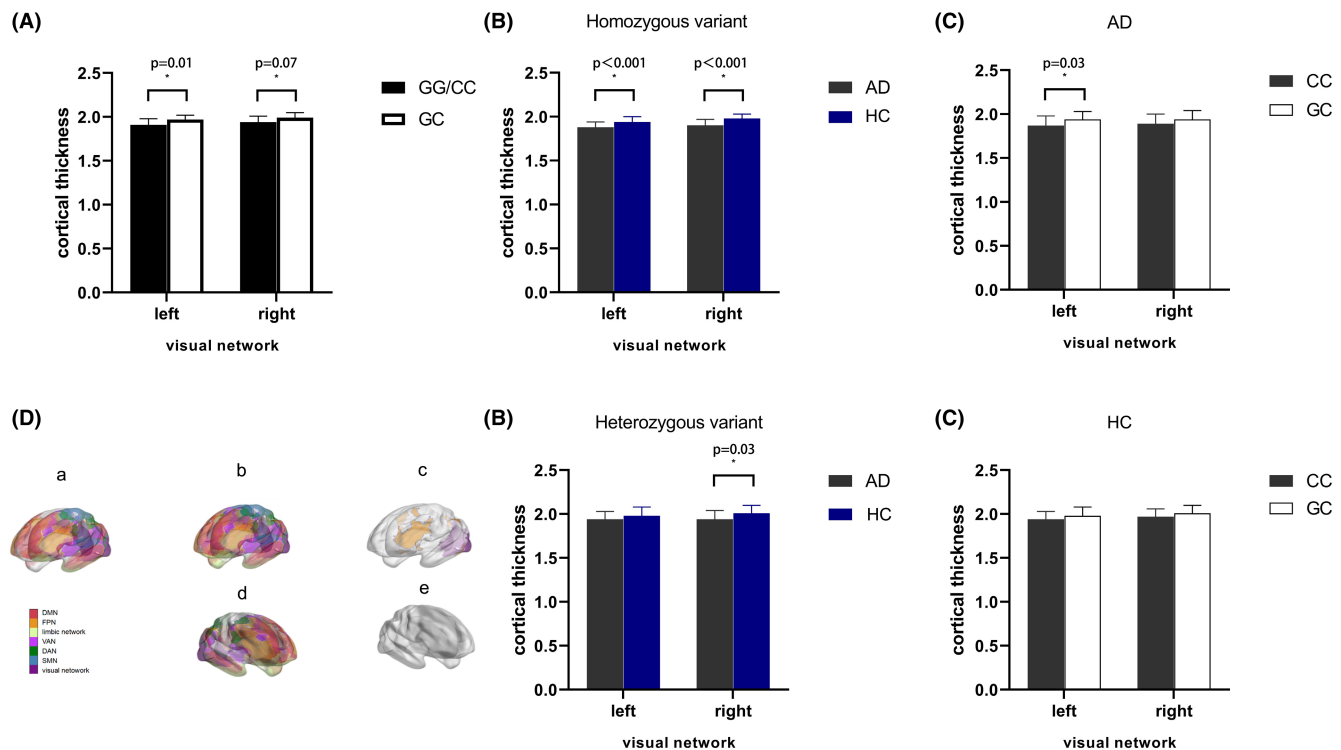
FIGURE 6 Results of the effects of TGM4 on cortical thickness-based visual network. (A) Both homozygous and heterozygous TGM4 caused cortical thickness atrophy of the visual network. (B) Among individuals with homozygous variants carrying the TGM4 gene, cortical thickness differed in both left and right visual network networks. Among individuals with heterozygous variants carrying the TGM4 gene, cortical thickness differed in the right visual network (C). In 149 AD (133 individuals with homozygous variant [CC] and 16 individuals with heterozygous variant [GC]), cortical thickness differed in the left visual network. In 179 HC (149 individuals with homozygous variants [CC] and 30 individuals with heterozygous variants [GC]), the statistical analysis results showed no significant difference in visual network cortical thickness. (D) Brain networks with significant differences besides the visual network. In Figure 6, a: Homozygous and heterozygous difference analysis. b: Differences between AD and HC brain networks in homozygous variants individuals. c: Differences between AD and HC brain networks in heterozygous variant individuals. d: Differences between homozygous variant and heterozygous variant brain networks in AD individuals. e: Differences between homozygous variant and heterozygous variant brain networks in HC individuals.

6 | CONCLUSIONS

Together, the present study strongly suggests that genetic coordinated changes in morphological features (cortical thickness and cortical surface) are biologically meaningful, thus potentially opening up a new window into our understanding of cortical organization in AD.

AUTHOR CONTRIBUTIONS

Haizhu Tan conceived and managed the project; Bo Sun pre-processed the imaging data, Jiahui Cai and Weixue Xiong contributed to data analysis, MD simulation, and performed the bioinformatics analysis; Xiaohui Zhu carried out the Co-IP experiments; Haizhu Tan, Jiahui Cai, Weixue Xiong, Xiaohui Zhu, Chengcheng Huang, Chiyu Wei, and Henghui Lin contributed to the writing of the drafts and the final version of the manuscript. All authors made critical contributions to the manuscript.

ACKNOWLEDGMENTS

FUNDING INFORMATION

CONFLICT OF INTEREST

The authors declare no competing interests.

DATA AVAILABILITY STATEMENT

The data used in this research were obtained from the ADNI database (http://adni.loni.usc.edu), an open-source database.

CONSENT TO PARTICIPATE

All consent documentations are available on the ADNI website (http://adni.loni.usc.edu/methods/documents/).

ORCID

Weixue Xiong https://orcid.org/0000-0002-2477-3695

REFERENCES

Andrews, T. J., Halpern, S. D., & Purves, D. (1997). Correlated size variations in human visual cortex, lateral geniculate nucleus, and optic tract. *Journal of Neuroscience, 17*, 2859–2868.

Avila Villanueva, M., Marcos Dolado, A., Gomez Ramirez, J., & Fernandez-Blazquez, M. A. (2022). Brain structural and functional changes in cognitive impairment due to Alzheimer's disease. *Frontiers in Psychology, 13*, 886619.

Bajaj, S., Alkozei, A., Dailey, N. S., & Killgore, W. D. (2017). Brain aging: Uncovering cortical characteristics of healthy aging in young adults. *Frontiers in Aging Neuroscience, 9*, 412.

Carlton, V. E., Ireland, J. S., Useche, F., & Faham, M. (2006). Functional single nucleotide polymorphism-based association studies. *Human Genomics, 2*, 1–12.

Chhatwal, J. P., Schultz, A. P., Johnson, K., Benzinger, T. L. S., Jack, C., Ances, B. M., Sullivan, C. A., Salloway, S. P., Ringman, J. M., Koeppe, R. A., Marcus, D. S., Thompson, P., Saykin, A. J., Correia, S., Schofield, P. R., Rowe, C. C., Fox, N. C., Brickman, A. M., Mayeux, R., … Sperling, R. A. (2013). Impaired default network functional connectivity in autosomal dominant Alzheimer disease. *Neurology, 81*, 736–744.

Chong, W. L., Chupradit, K., Chin, S. P., Khoo, M. M., Khor, S. M., Tayapiwatana, C., Nimmanpipug, P., Thongkum, W., & Lee, V. S. (2021). Protein-protein interactions: Insight from molecular dynamics simulations and nanoparticle tracking analysis. *Molecules, 26*, 5696.

de Jager, M., van der Wildt, B., Schul, E., Bol, J. G., van Duinen, S. G., Drukarch, B., & Wilhelmus, M. M. (2013). Tissue transglutaminase colocalizes with extracellular matrix proteins in cerebral amyloid angiopathy. *Neurobiology of Aging, 34*, 1159–1169.

Delbeuck, X., Van der Linden, M., & Collette, F. (2003). Alzheimer's disease as a disconnection syndrome? *Neuropsychology Review, 13*, 79–92.

Dominguez, C., Boelens, R., & Bonvin, A. M. (2003). HADDOCK: A protein– protein docking approach based on biochemical or biophysical information. *Journal of the American Chemical Society, 125*, 1731–1737.

Dudek, S. M., & Johnson, G. V. (1994). Transglutaminase facilitates the formation of polymers of the β-amyloid peptide. *Brain Research, 651*, 129–133.

Fagerholm, E. D., Hellyer, P. J., Scott, G., Leech, R., & Sharp, D. J. (2015). Disconnection of network hubs and cognitive impairment after traumatic brain injury. *Brain, 138*, 1696–1709.

Farris, F., Matafora, V., & Bachi, A. (2021). The emerging role of β-secretases in cancer. *Journal of Experimental & Clinical Cancer Research, 40*, 1–10.

Fauvel, B., Groussard, M., Chételat, G., Fouquet, M., Landeau, B., Eustache, F., Desgranges, B., & Platel, H. (2014). Morphological brain plasticity induced by musical expertise is accompanied by modulation of functional connectivity at rest. *NeuroImage, 90*, 179–188.

Gauch, H. G., Jr., Qian, S., Piepho, H.-P., Zhou, L., & Chen, R. (2019). Consequences of PCA graphs, SNP codings, and PCA variants for elucidating population structure. *PLoS One, 14*, e0218306.

Gentile, V., Grant, F., & Porta, R. (1995). Localization of the human prostate transglutaminase (type IV) gene (TGM4) to chromosome 3p21. 33-p22 by fluorescence in situ hybridization. *Genomics, 27*, 219–220.

Gopalakrishnan, C., Al-Subaie, A. M., Yeh, H. Y., Tayubi, I. A., & Kamaraj, B. (2019). Prioritization of SNPs in γ+ LAT-1 culpable of Lysinuric protein intolerance and their mutational impacts using protein-protein docking and molecular dynamics simulation studies. *Journal of Cellular Biochemistry, 120*, 18496–18508.

He, Y., Chen, Z., & Evans, A. (2008). Structural insights into aberrant topological patterns of large-scale cortical networks in Alzheimer's disease. *Journal of Neuroscience, 28*, 4756–4766.

Hollingsworth, S. A., & Dror, R. O. (2018). Molecular dynamics simulation for all. *Neuron, 99*, 1129–1143.

Honey, C. J., Kötter, R., Breakspear, M., & Sporns, O. (2007). Network structure of cerebral cortex shapes functional connectivity on multiple time scales. *Proceedings of the National Academy of Sciences of the United States of America, 104*, 10240–10245.

Hu, H., Li, H., Li, J., Yu, J., & Tan, L. (2018). Genome-wide association study identified ATP6V1H locus influencing cerebrospinal fluid BACE activity. *BMC Medical Genetics, 19*, 1–8.

Jellinger, K. A., & Attems, J. (2005). Prevalence and pathogenic role of cerebrovascular lesions in Alzheimer disease. *Journal of the Neurological Sciences, 229*, 37–41.

Keskin, O., Tuncbag, N., & Gursoy, A. (2016). Predicting protein–protein interactions from the molecular to the proteome level. *Chemical Reviews, 116*, 4884–4909.

Kim, M., Wu, R., Yao, X., Saykin, A. J., Moore, J. H., & Shen, L. (2022). Identifying genetic markers enriched by brain imaging endophenotypes in Alzheimer's disease. *BMC Medical Genomics, 15*, 1–12.

Laskowski, R. A., MacArthur, M. W., Moss, D. S., & Thornton, J. M. (1993). PROCHECK: A program to check the stereochemical quality of protein structures. *Journal of Applied Crystallography, 26*, 283–291.

Laurie, C. C., Doheny, K. F., Mirel, D. B., Pugh, E. W., Bierut, L. J., Bhangale, T., Boehm, F., Caporaso, N. E., Cornelis, M. C., Edenberg, H. J., Gabriel, S. B., Harris, E. L., Hu, F. B., Jacobs, K. B., Kraft, P., Landi, M. T., Lumley, T., Manolio, T. A., McHugh, C., … for the GENEVA Investigators. (2010). Quality control and quality assurance in genotypic data for genome-wide association studies. *Genetic Epidemiology, 34*, 591–602.

Martens, Y. A., Zhao, N., Liu, C.-C., Kanekiyo, T., Yang, A. J., Goate, A. M., Holtzman, D. M., & Bu, G. (2022). ApoE Cascade hypothesis in the pathogenesis of Alzheimer's disease and related dementias. *Neuron, 110*, 1304–1317.

Marwarha, G., Schommer, J., Lund, J., Schommer, T., & Ghribi, O. (2018). Palmitate-induced C/EBP homologous protein activation leads to NF-κB-mediated increase in BACE1 activity and amyloid beta genesis. *Journal of Neurochemistry, 144*, 761–779.

Palaniyappan, L., Al-Radaideh, A., Gowland, P. A., & Liddle, P. F. (2020). Cortical thickness and formal thought disorder in schizophrenia: An ultra high-field network-based morphometry study. *Progress in Neuro-Psychopharmacology and Biological Psychiatry, 101*, 109911.

Palk, A., Illes, J., Thompson, P. M., & Stein, D. J. (2020). Ethical issues in global neuroimaging genetics collaborations. *NeuroImage*, *221*, 117208.

Pettersen, E. F., Goddard, T. D., Huang, C. C., Couch, G. S., Greenblatt, D. M., Meng, E. C., & Ferrin, T. E. (2004). UCSF chimera—A visualization system for exploratory research and analysis. *Journal of Computational Chemistry*, *25*, 1605–1612.

Price, A. L., Patterson, N. J., Plenge, R. M., Weinblatt, M. E., Shadick, N. A., & Reich, D. (2006). Principal components analysis corrects for stratification in genome-wide association studies. *Nature Genetics*, *38*, 904–909.

Rostamirad, S. (2010). *Identification and characterization of a novel retinal protein, ANKRD33, and its interacting partner HPCAL-1*. University of British Columbia.

Rowe, T. W., Katzourou, I. K., Stevenson-Hoare, J. O., Bracher-Smith, M. R., Ivanov, D. K., & Escott-Price, V. (2021). Machine learning for the life-time risk prediction of Alzheimer's disease: A systematic review. *Brain Communications*, *3*, fcab246.

Stepler, K. E., Gillyard, T. R., Reed, C. B., Avery, T. M., Davis, J. S., & Robinson, R. A. (2022). ABCA7, a genetic risk factor associated with Alzheimer's disease risk in African Americans. *Journal of Alzheimer's Disease*, *86*, 1–15.

Tan, J. Z. A., Fourriere, L., Wang, J., Perez, F., Boncompain, G., & Gleeson, P. A. (2020). Distinct anterograde trafficking pathways of BACE1 and amyloid precursor protein from the TGN and the regulation of amyloid-β production. *Molecular Biology of the Cell*, *31*, 27–44.

Theocharis, A. D., Skandalis, S. S., Gialeli, C., & Karamanos, N. K. (2016). Extracellular matrix structure. *Advanced Drug Delivery Reviews*, *97*, 4–27.

Thiebaut de Schotten, M., Dell'Acqua, F., Forkel, S., Simmons, A., Vergani, F., Murphy, D. G., & Catani, M. (2011). A lateralized brain network for visuo-spatial attention. *Nature Neuroscience*, *14*, 1245–1246.

Thiebaut de Schotten, M., Foulon, C., & Nachev, P. (2020). Brain disconnections link structural connectivity with function and behaviour. *Nature Communications*, *11*, 1–8.

Van Den Heuvel, M. P., & Pol, H. E. H. (2010). Exploring the brain network: A review on resting-state fMRI functional connectivity. *European Neuropsychopharmacology*, *20*, 519–534.

Walker, R. L., Ramaswami, G., Hartl, C., Mancuso, N., Gandal, M. J., De La Torre-Ubieta, L., Pasaniuc, B., Stein, J. L., & Geschwind, D. H. (2019). Genetic control of expression and splicing in developing human brain informs disease mechanisms. *Cell*, *179*, 750–771.e22.

Wang, H., Bennett, D. A., De Jager, P. L., Zhang, Q.-Y., & Zhang, H.-Y. (2021). Genome-wide epistasis analysis for Alzheimer's disease and implications for genetic risk prediction. *Alzheimer's Research & Therapy*, *13*, 1–13.

Wang, Z., Huang, X., Zhao, P., Zhao, L., & Wang, Z.-Y. (2018). Catalpol inhibits amyloid-β generation through promoting α-cleavage of APP in Swedish mutant APP overexpressed N2a cells. *Frontiers in Aging Neuroscience*, *10*, 66.

Wen, C., Ba, H., Pan, W., Huang, M., & Alzheimer's Disease Neuroimaging Initiative. (2020). Co-sparse reduced-rank regression for association analysis between imaging phenotypes and genetic variants. *Bioinformatics*, *36*, 5214–5222.

Wiederstein, M., & Sippl, M. J. (2007). ProSA-web: Interactive web service for the recognition of errors in three-dimensional structures of proteins. *Nucleic Acids Research*, *35*, W407–W410.

Wilhelmus, M. M., De Jager, M., & Drukarch, B. (2012). Tissue transglutaminase: A novel therapeutic target in cerebral amyloid angiopathy. *Neurodegenerative Diseases*, *10*, 317–319.

Yang, H., Xu, H., Li, Q., Jin, Y., Jiang, W., Wang, J., Wu, Y., Li, W., Yang, C., Li, X., Xiao, S., Shi, F., & Wang, T. (2019). Study of brain morphology change in Alzheimer's disease and amnestic mild cognitive impairment compared with normal controls. *General Psychiatry*, *32*, e100005.

Yang, J., Yan, R., Roy, A., Xu, D., Poisson, J., & Zhang, Y. (2015). The I-TASSER suite: Protein structure and function prediction. *Nature Methods*, *12*, 7–8.

Ye, Q., Su, F., Shu, H., Gong, L., Xie, C. M., Zhou, H., Zhang, Z. J., & Bai, F. (2017). Shared effects of the clusterin gene on the default mode network among individuals at risk for Alzheimer's disease. *CNS Neuroscience & Therapeutics*, *23*, 395–404.

Yeo, B. T., Krienen, F. M., Sepulcre, J., Sabuncu, M. R., Lashkari, D., Hollinshead, M., Roffman, J. L., Smoller, J. W., Zöllei, L., Polimeni, J. R., Fischl, B., Liu, H., & Buckner, R. L. (2011). The organization of the human cerebral cortex estimated by intrinsic functional connectivity. *Journal of Neurophysiology*, *106*, 1125–1165.

Yi-Bin, W., Xiang, L., Bing, Y., Qi, Z., Fei-Tong, J., Minghong, W., Xiangxiang, Z., Ie, K., Yan, L., Ping, S., Yufei, G., Ye, X., & Chun-Yan, W. (2022). Inhibition of the CEBPβ-NFκB interaction by nanocarrier-packaged Carnosic acid ameliorates glia-mediated neuroinflammation and improves cognitive function in an Alzheimer's disease model. *Cell Death & Disease*, *13*, 1–18.

Zamora-López, G., Zhou, C., & Kurths, J. (2011). Exploring brain function from anatomical connectivity. *Frontiers in Neuroscience*, *5*, 83.

Zhang, X., & Song, W. (2013). The role of APP and BACE1 trafficking in APP processing and amyloid-β generation. *Alzheimer's Research & Therapy*, *5*, 1–8.

Zhao, B., Li, T., Smith, S. M., Xiong, D., Wang, X., Yang, Y., Luo, T., Zhu, Z., Shan, Y., Matoba, N., Sun, Q., Yang, Y., Hauberg, M. E., Bendl, J., Fullard, J. F., Roussos, P., Lin, W., Li, Y., Stein, J. L., & Zhu, H. (2022). Common variants contribute to intrinsic human brain functional networks. *Nature Genetics*, *54*, 508–517.

Zicha, S., Bateman, R. J., Shaw, L. M., Zetterberg, H., Bannon, A. W., Horton, W. A., Baratta, M., Kolb, H. C., Dobler, I., Mordashova, Y., Saad, Z. S., Raunig, D. L., Spanakis, E. M., Li, Y., Schindler, S. E., Ferber, K., Rubel, C. E., Martone, R. L., Weber, C. J., ... Foundation for the National Institutes of Health (FNIH) Biomarkers Consortium Plasma Aβ as a Predictor of Amyloid Positivity in Alzheimer's Disease Project Team. (2022). Comparative analytical performance of multiple plasma Aβ42 and Aβ40 assays and their ability to predict positron emission tomography amyloid positivity. *Alzheimer's & Dementia*, *2022*, alz.12697.

SUPPORTING INFORMATION

Additional supporting information can be found online in the Supporting Information section at the end of this article.